



A Novel Mitochondrial-Related Gene Signature for the Prediction of Prognosis and Therapeutic Efficacy in Lower-Grade Glioma

Jingyi Yang¹ · Lei Shen¹ · Jiaxin Zhou¹ · Ji Wu¹ · Chuqiao Yue¹ ·
Tiansheng Wang¹ · Songshan Chai¹ · Yuankun Cai¹ · Dongyuan Xu¹ · Yu Lei¹ ·
Jingwei Zhao¹ · Yixuan Zhou¹ · Zhimin Mei¹ · Nanxiang Xiong¹

Received: 16 March 2024 / Accepted: 15 September 2024

© The Author(s), under exclusive licence to Springer Science+Business Media, LLC, part of Springer Nature 2024

Abstract

Lower-grade glioma (LGG) is a common primary brain tumor with a highly heterogeneous clinical presentation, and its prognosis cannot be accurately predicted by current histopathology. It has been found that mitochondria play an important role in hypoxia, angiogenesis, and energy metabolism in glioma, and mitochondrial function may have an important impact on LGG prognosis. The goal of this study was to develop a novel prognostic model based on Mitochondrial-related genes (MRGs). We first analyzed the somatic alterations profiles of MRGs in patients with LGG and found that somatic alterations were common in LGG and correlated with prognosis. Using RNA-seq data from TCGA and CGGA, 12 prognosis-related MRGs were identified to construct a mitochondrial activation score (MiAS) model by combining univariate regression and LASSO regression analysis. The model and nomogram were evaluated using the area under the ROC curve with AUC=0.910. The model was closely correlated with the clinical characteristics of LGG patients and performed well in predicting the prognosis of LGG patients with significantly shorter overall survival (OS) time in the high-MiAS group. GSVA and GSEA results showed that oxidative stress, pro-cancer, and immune-related pathways were significantly enriched in the high-MiAS group. CIBERSORT results showed that MiAS was significantly associated with immune cell infiltration in LGG. Macrophage M1 and follicular helper T cells had increased infiltration in the high-MiAS group. TIDE predicted a better immunotherapy outcome in patients in the low-MiAS group. Finally, using data from the CTRPv2 and GDSC2 datasets to assess chemotherapy response in LGG, it was predicted that the chemotherapeutic agents AZD6482, MG-132, and PLX-4720 might be potential agents for patients in the high-MiAS group of LGG. In addition, we performed in vitro experiments and

Jingyi Yang and Lei Shen contributed equally to this work.

Extended author information available on the last page of the article

found that knockdown of OCIAD2 expression reduced the abilities of glioma cells to proliferate, migrate, and invade. In contrast, overexpression of OCIAD2 enhanced these abilities of glioma cells. This study found that MRGs were correlated with LGG patient prognosis, which is expected to provide new treatment strategies for LGG patients with different MiAS.

Keywords Lower-grade glioma · Mitochondrial-related genes · Prognosis · Therapeutic efficacy · OCIA domain containing 2

Background

Glioma is the most common primary intracranial tumor, and lower-grade glioma (LGG) is one of the important types (Lapointe et al. 2018), and surgical resection combined with postoperative radiotherapy is currently the standard treatment for LGG (Soffietti et al. 2010). The World Health Organization Classification of Tumors of the Central Nervous System, 5th edition, 2021 (WHO CNS 5) states that glioma molecular biomarkers and genetic testing can help to classify glioma and provide targets and research directions for precise treatment, especially pointing out the importance of molecular diagnosis (Louis et al. 2021).

In recent years, an increasing number of glioma-related studies have shown that mitochondrial abnormalities such as abnormal mitochondrial structure, mutations in the mtDNA genome, altered energy metabolism (Warburg effect), and isocitrate dehydrogenase (IDH) mutations are extremely common in gliomas (Ordys et al. 2010; Liang and Hays 1996; Poff et al. 2019; Yan et al. 2009). For example, elevated mitochondrial transcription elongation factor (TEFM) expression predicts poor prognosis in LGG (Li et al. 2020), and glutathione peroxidase 1 (GPX1) is a prognostic and chemotherapy-related biomarker for LGG (Chen et al. 2022). However, mitochondrial-related studies of LGG are scarce and focused on the function of individual genes, and no studies have systematically explored the molecular characteristics and prognostic potential of mitochondrial-related genes (MRGs) using gene expression profiling data.

Due to the great heterogeneity of LGGs, some of them grow slowly and have a good prognosis, while others may recur and rapidly proliferate and invade to develop into higher grade gliomas (Bent 2010; Schiff et al. 2019). Surgical resection cannot completely solve the problem of tumor cells invading normal neuronal tissues. For example, total resection is often not possible for tumors invading functional areas, and immunotherapy is gradually becoming a new idea for its treatment. Many studies have focused on the tumor immune microenvironment (TIME) and the interaction between the tumor and immune cells. However, research on LGG immunotherapy is still to be further developed. The role of mitochondria in tumor immune escape and the effect of mitochondria-targeted anti-tumor therapy have been demonstrated (Klein et al. 2020). Finding more precise targets for the further development of LGG immunotherapy based on MRGs will improve the treatment outcome of LGG patients.

In this study, we extracted RNA sequencing and clinical data of LGG patients from the Cancer Genome Atlas (TCGA) database to construct a novel Mitochondrial Activation Score (MiAS) prognostic model to explore the prognostic value of MRGs in LGG patients, further identify LGG molecular subtypes and discover novel immunotherapeutic targets. It is of great clinical significance for personalizing the treatment of LGG patients.

Materials and Methods

Data and Gene Collection

RNA sequencing data of 498 LGGs and corresponding clinical information were obtained from the TCGA (<https://portal.gdc.cancer.gov/>) database. Meanwhile, RNA sequencing data and clinical data of 271 LGG patients were obtained from the China Glioma Genome Atlas (CGGA, <http://www.cgga.org.cn/>) as an external validation set (Zhao et al. 2021). A total of 1136 MRGs were collected from the Human Mitochondrial Genome Database (MITOMAP, <http://www/MITOMAP.org>) for subsequent analysis (Supplementary file 1). In addition, a data set on atezolizumab, an anti-programmed death ligand 1 (PD-L1) monoclonal antibody for the treatment of uroepithelial carcinoma, was obtained from the IMvigor210 dataset to assess the predictive value of the MRGs signature on the efficacy of immunotherapy (Rosenberg et al. 2016). The clinical characteristics of LGG patients included in the study are shown in Table 1.

Somatic Alteration Analysis

The single nucleotide polymorphism (SNP) and copy number variation (CNV) data of LGG patients in TCGA were obtained from the UCSC Xena database (<https://xenabrowser.net/>). The copy number value of each gene was normalized and estimated by GISTIC2 (<https://broadinstitute.github.io/gistic2/>). A gene is considered to have copy number gain if the copy number value of this gene is greater than 0.3, and copy number loss if less than 0.3. The expression and CNV alteration status of MRGs in LGG patients were presented as a chromosome circle plot using R package “RCircos.” We also studied the relationship between the somatic alterations status of MRGs and the prognosis of LGG patients.

Construction and Validation of the Prognostic Models

The MRGs most associated with prognosis were obtained by univariate Cox regression analysis and least absolute shrinkage and selection operator (LASSO) regression analysis. MiAS was calculated based on the formula (Wang et al. 2021): $MiAS = ((Gene1_{HR>1} + Gene2_{HR>1} + \dots + GeneN_{HR>1}) - (Gene1_{HR<1} + Gene2_{HR<1} + \dots + GeneN_{HR<1})) * (PC1 + PC2)$. Patients were divided into high-MiAS and low-MiAS groups according to MiAS. Kaplan–Meier curves were plotted using the

Table 1 Clinical characteristics of patients in the dataset

	TCGA (<i>n</i> =498)	CGGA (<i>n</i> =271)	<i>p</i> value
<i>Age</i>			
>40	255	130	0.287
≤40	243	140	
NA	0	1	
<i>Gender</i>			
Male	277	151	0.979
Female	221	120	
<i>Histologic grade</i>			
WHO II	240	130	0.956
WHO III	258	141	
<i>IDH Mutation</i>			
Mutant	399	176	0.008
Wildtype	90	65	
NA	9	30	
<i>1p/19q Codelet^a</i>			
Codelet	161	81	0.795
Noncodelet	328	158	
NA	9	32	

IDH isocitrate dehydrogenase, *WHO* World Health Organization, *NA* not available

p value, significant difference between the TCGA dataset and the CGGA dataset

^a1p/19q co-deletion status

“survminer” and “Survival” packages. The receiver operating characteristic (ROC) curves were used to assess the accuracy and prognostic value of MRGs-based prognostic signature. In addition, the CGGA dataset was used as an external dataset to further validate the predictive power of the prognostic signature.

Subgroup Analysis of Clinical Characteristics

Subgroup analysis was performed to confirm the correlation between MiAS and clinical characteristics. Based on the available clinical data, patients were divided into several subgroups of age (≤40 and >40 groups), gender (male and female groups), tumor grade (WHO II and WHO III groups), IDH mutation status (IDH wildtype and IDH mutant groups), and 1p/19q co-deletion status (co-deletion and non-co-deletion groups) and the differences in MiAS between groups were compared. Meanwhile, considering the influence of clinical characteristics on patients’ prognosis, we integrated patients’ clinical characteristics with MiAS to further construct a clinical prognostic model. The R packages “rms” (<https://cran.r-project.org/web/packages/rms/>) and “regplot” (<https://cran.r-project.org/web/packages/regplot/>) were used to construct and visualize the nomogram and calibration curves.

Enrichment Analysis

Gene set enrichment analysis (GSEA) (Subramanian et al. 2005) was used for enrichment analysis based on the pathways from Gene Ontology (GO) (Gene ontology consortium: going forward 2015) terminology and Kyoto Encyclopedia of Genes and Genomes (KEGG) (Kanehisa and Goto 2000) pathways, and each LGG sample was scored using Gene Set Variance Analysis (GSVA) (Hanzelmann et al. 2013).

Evaluation of Immune Cell Infiltration and Immunotherapy

We investigated the relationship between the level of LGG immune infiltration in the high- and low-MiAS groups. Stromal score, immune score, ESTIMATE score, and tumor purity were calculated using Estimation of STromal and Immune cells in MAlignant Tumor tissues using Expression data (ESTIMATE) to analyze the estimation of stromal and immune cells in malignant tumor tissues and to clarify the difference between the tumor microenvironment in the high- and low-MiAS groups (Yoshihara et al. 2013). Tumor immune cell infiltration was analyzed by the CIBERSORT method (Newman et al. 2015). The efficacy of immune checkpoint inhibitors (ICIs) in LGG patients was evaluated based on tumor immune dysfunction and exclusion (TIDE) prediction of immunotherapy response simulating tumor immune escape mechanisms (Benitez et al. 2020).

Potentially Sensitive Drug Prediction and Chemotherapy Efficacy Evaluation

Drug sensitivity data from the Genomics of Drug Sensitivity in Cancer (GDSC, <https://www.cancerrxgene.org/>) (Yang et al. 2013) and the Cancer Therapy Response Portal (“CTRP v2” dataset <https://portals.broadinstitute.org/ctrp>) (Seashore-Ludlow et al. 2015) datasets and cell line expression data from the Cancer Cell Line Encyclopedia (CCLE) (Ghandi et al. 2019) were obtained to predict potentially sensitive drugs in the high-MiAS and low-MiAS groups. The sensitivity scores of each sample in this study were predicted by the R package “oncoPredict” (Maeser et al. 2021). The sensitivity of the glioma cells to the drug was determined using a sensitivity score, with lower sensitivity scores indicating greater sensitivity to the potential drug.

Cell Culture and Transfection

Glioma cell lines including A172 and U251 were purchased from the Chinese Academy of Sciences Cell Bank (Shanghai, China) and cultured in complete medium (Dulbecco’s modified Eagle medium (DMEM; Servicebio) with 10% fetal bovine serum (FBS, Gibco) and 10 µl/ml penicillin–streptomycin (Biosharp)) and incubated in a humidified chamber at 37 °C with 5% CO₂.

Lentiviral vectors based on the sense sequence of short hairpin (sh) RNA against human OCIAD2 (5'-GCGUCUGCUCGUGUGGAAACCAAGAUA-3'), negative control shRNA (5'-UUCUCCGAACGUGUCACGU-3'), and lentiviruses overexpressing OCIAD2 were obtained from GeneChem Biotech (Shanghai, China). Lentiviral infection was performed according to the protocol provided by the manufacturer. First, 5×10^4 glioma cells were inoculated into each well of a 12-well plate and cultured overnight in DMEM containing 10% FBS and 10 μ l/ml penicillin-streptomycin, with approximately 30% confluence. After overnight, each well was infected for 16 h by adding 10 μ l of 1×10^8 TU/ml virus solution and 40 μ l of 25 \times HitransG P infection solution to the medium. After 16 h of infection, the medium was changed to DMEM containing 10% FBS and 10 μ l/ml penicillin-streptomycin. Finally, glioma cells infected with lentiviruses containing shRNA and lentiviruses overexpressing OCIAD2 were cultured for 48–72 h. When green fluorescence was visible under the microscope and the abundance of fluorescent expression was high (about 80%), the cells were screened by adding puromycin at 2 μ g/ml for 48 h. After 48 h, quantitative real-time PCR (qPCR) was performed to identify the knockdown and overexpression efficiencies of OCIAD2 in the cells, and the cells were used for further experiments.

RNA Extraction, cDNA Synthesis, and qPCR

Takara RNAiso Plus (Takara Bio. Inc., Otsu, Shiga, Japan) was used to extract total RNA from the glioma cells according to the manufacturer's protocol. The specific steps for extracting RNA are as follows: (1) Collect cells from culture plate with 1 ml RNase-free water. (2) Spin down cells at 4000 \times g in microfuge for 1 min. (3) Remove excess water and add 1 ml Trizol reagent. Vortex and invert tube. Stand it at room temperature for 10 min. (4) Spin tubes in microfuge at 12,000 rpm for 10 min at 4 °C. (5) Remove supernatant into fresh RNase-free eppendorf tube and add 200 μ l of chloroform. (6) Vortex for 15 s and let sit at room temperature for 5 min. (7) Spin in microfuge at 12,000 rpm for 15 min at 4 °C. (8) Transfer the supernatant into a new RNase-free eppendorf tube and add 500 μ l of Isopropanol. Invert to mix. Stand it for 10 min at room temperature. (9) Spin in microfuge at 12,000 rpm for 10 min at 4 °C. (10) Remove the supernatant and wash RNA pellet with 100 μ l of 75% ethanol (made by diluting into DEPC-treated water). (11) Spin in microfuge at 7500 \times g for 5 min at 4 °C. (12) Remove supernatant and air dry pellet for 5 min. (13) Dissolve RNA pellet in 20 μ l of DEPC-treated water. The cDNA was synthesized from 250 ng RNA according to the HiScriptIIQ RT SuperMix for qPCR Kit (Vazyme Medical Technology, Nanjing, China). The $2 - \Delta Ct$ method was used to process qPCR data as follows. Firstly, export the Ct value data from the real-time PCR machine at the maximum curvature of the quantification curve. Then the delta Ct of each sample was calculated by subtracting the Ct value of GAPDH from the Ct value of the interest gene. The $\Delta\Delta Ct$ of each sample was calculated by subtracting the ΔCt value of one control sample from the Ct value of one experimental sample. Finally, the relative gene expression of the interest gene of experimental samples compared to the control samples was calculated by taking the log base 2 for minus

$\Delta\Delta Ct$. Primer sequences used are listed as follows: GAPDH-F, 5'-GGAGCGAGA TCCCTCCAAAAT-3', GAPDH-R, 5'-GGCTGTTGTACACTTCTCATGG-3'; OCIAD2-F, 5'-TGCTTGTACCCAGGGACTA-3', OCIAD2-R, 5'-CCTCACAGG TAAGGAGGCAGT-3'.

Cell Counting Kit-8 Proliferation Assay

Cell counting Kit-8 (CCK8) assay was conducted to evaluate cell proliferation ability according to the manufacturer's protocol (A311-01, Vazyme Biotech, Nanjing, China). Firstly, A172 and U251 cells were seeded at a density of 5000 cells/100 μ l/well and cultured in 96-well plates for 72 h. Then, 10 μ l of CCK8 solution was added to each well of the plates and incubated for 2 h at 37 °C. Finally, the optical density (OD) value was measured at 450 nm by using a BioTek Synergy HT Microplate Reader. Since the OD value was linearly related to the number of cells, we used the OD value to estimate the effect of transfected siRNA on the proliferation ability of glioma cells.

Colony Formation Assay

For the colony formation assay, 500 glioma cells were seeded into 6-well plates with three repetitions. After a 14-day incubation, when the colonies were visible to the naked eye, these plates were washed with PBS twice, fixed by 4% paraformaldehyde (Servicebio, Wuhan, China) for 30 min and stained with 0.1% crystal violet solution (Servicebio, Wuhan, China) for 15 min. Then, the colony assay was photographed for further analysis.

Transwell

In the transwell assay, 10,000 glioma cells were seeded into transwell chambers coated with matrix gel with three repetitions. After 48 h of incubation, the cells were rinsed three times with calcium-free PBS (Servicebio, Wuhan, China). The upper layer of remaining cells was wiped away as much as possible with cotton swabs. The chambers were fixed with 4% paraformaldehyde (Servicebio, Wuhan, China) for 30 min and stained with 0.1% crystal violet solution (Servicebio, Wuhan, China) for 15 min. Then, the chambers were observed and photographed under a microscope.

Wound Healing Assay

The wound healing assay was performed to evaluate cell migration ability. A172 and U251 cells were seeded in 6-well plates at a density of 500,000 cells/ml/well. After cultured for 24 h, a 10 μ l disposable pipette tip was run over the surface of the cells to create wounds. The cells were washed three times with phosphate buffered saline (PBS) and cultured in 3% FBS (low concentration) medium to reduce the interference of cell proliferation on the results. The extent of wound healing was measured at 0 and 48 h, respectively, using a microscope.

Statistical Analysis

Statistical analyses and visualizations were performed using R version 4.1.3(<https://rstudio.com/>). Correlations between MiAS and other characteristics were determined using Spearman correlation analysis. The Student's t test was used to compare the differences between the two groups following the normal distribution. The Wilcoxon rank-sum test was used to identify differentially expressed genes and differences between the two groups not following the normal distribution. The Chi-square test was used to determine whether the clinical characteristics between the training and validation sets were different. Kaplan–Meier analysis was used to compare the differences in survival between the two groups. Univariate Cox analysis was used to assess the effect of variables on prognosis. The predictive value of the risk scores was assessed using a time-dependent ROC curve analysis. Two-sided $p \leq 0.05$ (*) was considered statistically significant and was further stratified to $p < 0.01$ (**), $p < 0.001$ (***) $, and p < 0.0001$ (****).

Results

Somatic Alteration Landscape of MRGs in LGG

To explore the genomic features of MRGs in LGG, we visualized the CNV mutation status of MRGs in 533 LGG patients in the TCGA cohort (Fig. 1A). The lolipop chart showed the CNV frequency of the top 20 MRGs (Fig. 1B). CNV losses occurred more frequently than CNV gains in MRGs in LGG patients, and the top 5 MRGs with the highest CNV loss incidence were ISOC2 (12.57%), COX6B2 (12.57%), RDH13 (12.20%), NDUFA3 (12.01%), and ETFB (10.88%). The SNP events of MRGs occurred in 49.72% of LGG patients, with a mutation frequency ranging from 1 to 4%. The MRGs with the highest mutation frequency were IDH2 (4%), ACACA (2%), and ACACB (2%) (Fig. 1C). The most frequent base alteration was C to T mutation (Fig. 1D). 86.87% of LGG patients had somatic alterations of MRGs, and the most frequent SNP event was missense mutation (78.88%) (Fig. 1E). The somatic alteration status of MRGs was also correlated with the prognosis of LGG patients, patients with both CNV and SNP mutations had worse prognosis ($p=0.036$) (Fig. 1F). In summary, somatic alterations of MRGs are common in LGG and are associated with the prognosis of LGG patients.

Construction of a Novel Prognostic Signature Based on MRGs for LGG

Univariate Cox regression analysis was performed to analyze the correlation between the expression of MRGs and the OS of LGG patients in the TCGA dataset, and 113 prognostically relevant MRGs were identified (Supplementary file 2). LASSO analysis was performed on 113 MRGs (Fig. 2A, B). 12 MRGs (GCAT, SLC25A45, ACSL6, ACSM3, UNG, OCIAD2, POLQ, CYP24A1, COMTD1,

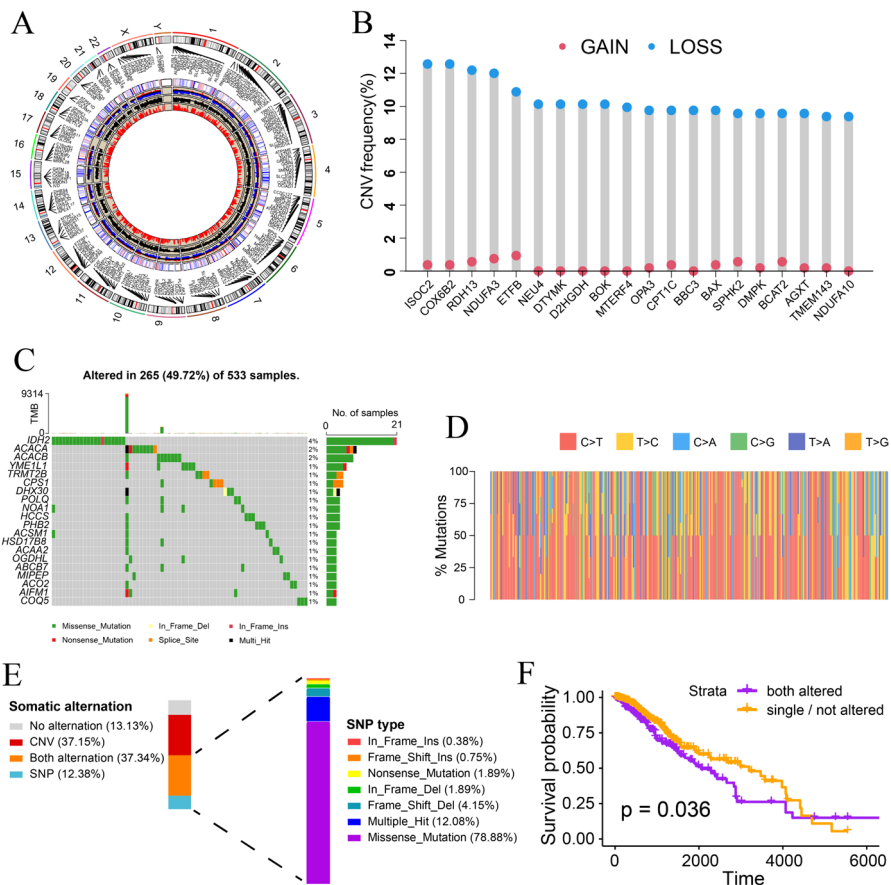


Fig. 1 The CNV and SNP landscape of MRGs in LGG **A** chromosome circle plot of CNV of MRGs in LGG patients **B** lollipop chart of the top 20 MRGs with the highest CNV loss **C** oncoplot of SNP of top 20 MRGs in LGG **D** stacked histogram of SNP base alterations in LGG patients **E** stacked histogram of the proportion of somatic alterations and SNP in LGG patients **F** KM curve of patients with and without both somatic alterations

CYP27B1, MGME1, PRSS35) that were strongly correlated with OS were further screened. The correlation of these 12 MRGs with the prognosis of LGG patients was consistent in the TCGA dataset and the CGGA dataset (Fig. 2C, D). A prognostic signature was constructed using the MiAS, and 498 patients in the TCGA dataset were divided into a high-MiAS group and a low-MiAS group. The Kaplan–Meier method was used to analyze the OS of patients in both groups, and the results showed that patients in the high-MiAS group had significantly shorter OS in TCGA ($p < 0.0001$) (Fig. 3A). The MiAS, OS, and survival status distribution of LGG patients are shown in Fig. 3B. Based on ROC curve analysis, we evaluated the predictive performance and accuracy of prognostic characteristics at 1, 3, and 5 years. The signatures had predicted area under the ROC curve (AUC) values of 0.910, 0.867, and 0.802 at 1, 3, and 5 years, respectively (Fig. 3C). 7 of the 12 MRGs,

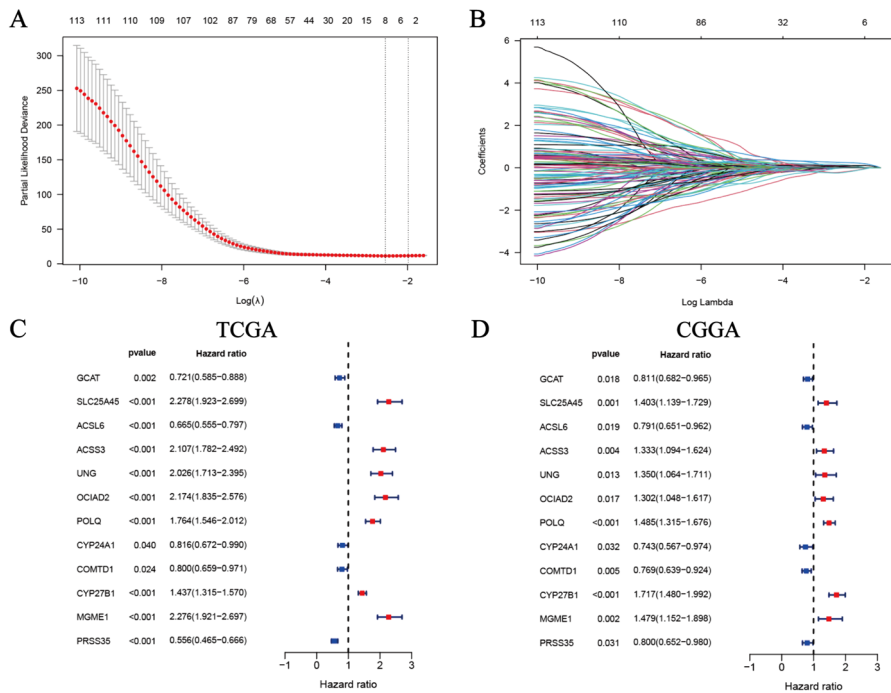


Fig. 2 Construction of the signature **A, B** LASSO analysis **C** The forest plot of 12 MRGs in the TCGA dataset **D** The forest plot of 12 MRGs in the CGGA dataset

including ACSS3, OClAD2, SLC25A45, CYP27B1, UNG, POLQ, and MGME1, were highly expressed in the high-MiAS group in TCGA (Fig. 3D). Next, the stability and applicability of the prognostic characteristics were assessed according to the CGGA external validation dataset. The results of Kaplan–Meier survival analysis were consistent with the above results ($p < 0.0001$) (Fig. 3E). Similar to the TCGA dataset, patients in the high-MiAS group in CGGA had a shorter overall survival time, high expression of 7 of the 12 MRGs in the signature, and censored status was enriched in the high-MiAS group (Fig. 3F, H). Based on the CGGA dataset, the AUC predictive values of the signature at 1, 3, and 5 years were 0.713, 0.788, and 0.754, respectively (Fig. 3G). Therefore, there is sufficient evidence for the good stability and predictive performance of the MRGs-based predictive signature in this study.

Construction of Clinical Prediction Models Based on MiAS and Clinical Characteristics

Among the available subgroups of clinical features, the signature showed accurate and stable performance. MiAS was significantly elevated in patients with age > 40 years ($p < 0.0001$), WHO III ($p < 0.0001$), isocitrate dehydrogenase (IDH) wild type ($p < 0.0001$), and 1p/19q non-co-deletion ($p < 0.0001$) in TCGA (Fig. 4A).

The relationship between clinical characteristics and MiAS in the validation set showed no statistically significant differences in age and grading between the two groups ($p > 0.05$), while the same trend as in the training set ($p < 0.0001$) was observed for group differences in IDH mutations and 1p/19q co-deletions (Fig. 4B). Subsequently, nomogram models based on the TCGA and CGGA datasets were constructed with high accuracy in predicting the prognosis of LGG patients (Fig. 4C, D, F, G), and the AUCs for predicting 1-year, 3-year, and 5-year survival of LGG patients were 0.868, 0.900, and 0.838 in the TCGA dataset (Fig. 4E) and 0.836, 0.851, and 0.796 in the CGGA dataset, respectively (Fig. 4H).

Enrichment Analysis Between the High- and Low-MiAS Groups

We performed GSVA and GSEA between the high- and low-MiAS groups to assess the involvement of biological processes in each LGG sample and identified relevant molecular functions and crucial signaling pathways. GSEA showed that in the high-MiAS group of the TCGA dataset, antigen processing presentation, Fc ϵ RI signaling pathway, Fc γ R-mediated phagocytosis, human immunodeficiency virus type 1 infection, leukocyte transendothelial cell migration, apoptosis, JAK-STAT signaling pathway, MAPK signaling pathway, NOD-like receptor signaling pathway, and T-cell receptor signaling pathway were increased in the KEGG pathways (Fig. 5A, B). Figure 6A, B shows the GO terms enriched in the high-MiAS group of the TCGA dataset, including Fc- γ receptor signaling pathway, Fc receptor-mediated stimulatory signaling pathway, MHC class II protein complex binding, MHC protein complex binding, response to interferon- β , cellular response to oxidative stress, cellular response to reactive oxygen species, cellular senescence, regulation of cellular response to oxidative stress, regulation of protein autophosphorylation, and response to hydrogen peroxide. The KEGG pathways and GO terms enriched in the TCGA dataset were also enriched in the high-MiAS group of the CGGA dataset (Figs. 5C, D and 6C, D). The GSVA results showed that in the high-MiAS group of both the TCGA and CGGA datasets, the P53 signaling pathway, adherent spots, apoptosis, B-cell receptor signaling pathway, T-cell receptor signaling pathway, and Toll-like receptor signaling pathway were significantly enriched (Fig. 5E, F), while Fig. 6E, F shows the top 15 GO terms enriched in the high-MiAS group versus the low-MiAS group for the TCGA and CGGA datasets, respectively. These results suggest that the prognostic MRGs may play an important role by influencing the immune microenvironment, redox homeostasis, signaling, and metastasis mechanisms of LGG.

Immune Infiltration Analysis

This study identified significant differences in immune cell infiltration and immunotherapy response rates between the high- and low-MiAS groups. ESTIMATE analysis showed that ESTIMATE scores, immune and stromal scores were positively correlated with MiAS, and lower tumor purity was negatively correlated with MiAS in TCGA (Fig. 7A). The samples in the CGGA dataset had the same trend (Fig. 7B).

Fig. 3 Prognostic value of MRGs-based signature based on TCGA and CGGA datasets **A** Kaplan–Meier ► survival curve analysis for overall survival grouped by the median MiAS in the TCGA dataset **B** Distribution of the MiAS, overall survival, and survival status of the prognostic signature in the TCGA dataset **C** Time-dependent ROC curves measuring the predictive value of the MiAS in the TCGA dataset **D** Heatmap showing the expression of 12 MRGs in the TCGA dataset **E** Kaplan–Meier survival curve analysis for overall survival grouped by the median MiAS in the CGGA dataset **F** Distribution of the MiAS, overall survival, and survival status of the prognostic signature in the CGGA dataset **G** Time-dependent ROC curves measuring the predictive value of the MiAS in the CGGA dataset **H** Heatmap showing the expression of 12 MRGs in the CGGA dataset

CIBERSORT analysis showed significant differences in immune infiltration between the high- and low-MiAS groups. The TCGA dataset and CGGA dataset consistently showed significantly increased infiltration of M1 macrophages and follicular helper T cells in the high-MiAS group, in addition to significantly enriched B-cell plasma and T-cell CD4 naïve in the low-MiAS group (Fig. 7C–F).

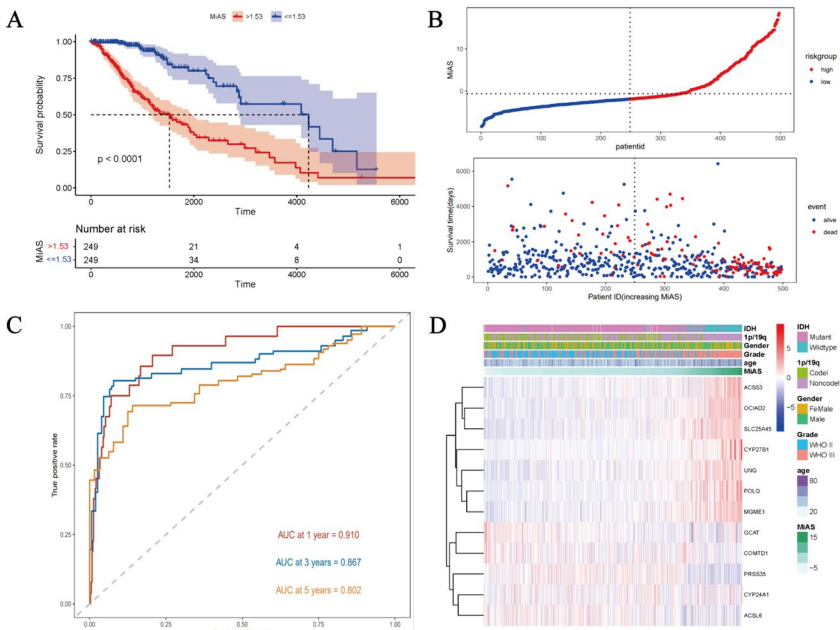
Immunotherapy Analysis

The TIDE-based algorithm to predict the likelihood of immunotherapy response in LGG patients in the TCGA dataset showed that as patient MiAS scores increased, TIDE scores ($R=0.31$, $p=3.4e-12$) and cancer-associated fibroblast infiltration (CAF) in LGG patients ($R=0.54$, $p<2.2e-16$) increased (Fig. 8A). The same trend was observed in the CGGA dataset (Fig. 8B). Since a high TIDE score indicates a poor response to ICIs, our study showed that the low-MiAS group had a significantly lower TIDE score and a better response to ICIs. By comparing the common immune checkpoints between the high- and low-MiAS groups in LGG, the expression of several immune checkpoints was significantly higher in the high-MiAS group than in the low-MiAS group in both TCGA and CGGA, such as CD274, CD80, IDO1, HAVCR2, RASA2, ICOSLG, CTLA4, ICOS, CD28, BTLA, PDCD1, PDCD1LG2 ($p<0.001$) (Fig. 8C, D). To further validate the correlation between the 12 MRGs signature and the efficacy of immunotherapy, we extracted data from the IMvigor210 dataset for a group of patients receiving atezolizumab for uroepithelial cancer. The results showed that the 12 MRGs signature was significantly correlated with survival in patients with uroepithelial carcinoma treated with atezolizumab ($p=0.011$) (Fig. 8E).

Sensitivity Drug Prediction

The responses of the high-MiAS and low-MiAS groups in the TCGA dataset differed for 400 drugs in the CTRP v2 dataset and 100 drugs in the GDSC2 dataset, and 485 drugs in the CTRP v2 dataset and 177 drugs in the GDSC2 dataset in the CGGA dataset, and eight overlapping drugs were obtained from the intersection set for further analysis (Fig. 9A). Three drugs (AZD6482, MG-132, and PLX-4720) were identified as potential drugs by spearman correlation analysis, and the sensitivity of the samples to drugs in the CTRP v2 dataset was consistent with the trend in the GDSC2 dataset in the TCGA and CGGA datasets (Fig. 9B–I), and the

TCGA



CGGA

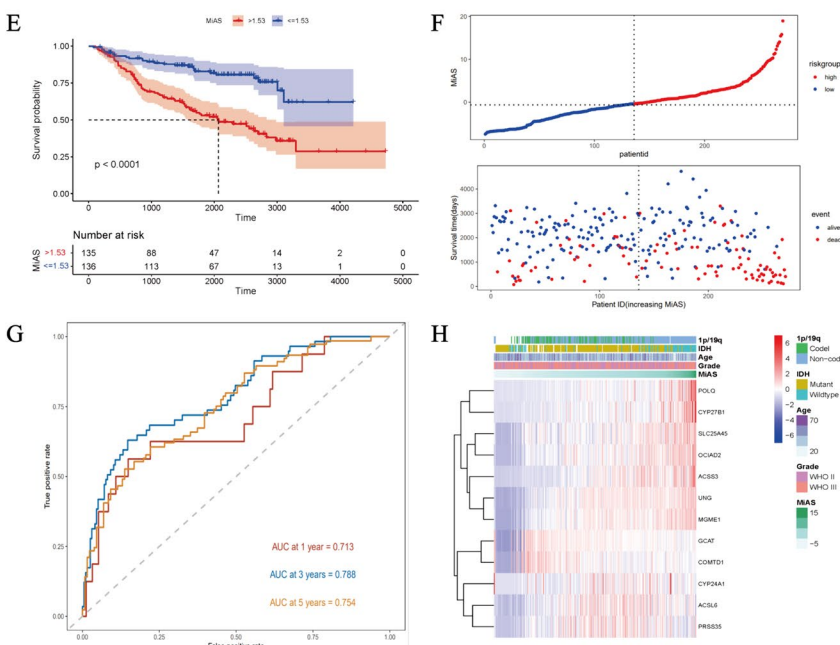


Fig. 4 Association analysis between the MRGs signature and clinical features and establishment of a ▶ nomogram **A** Subgroup analysis of clinical characteristics: Subgroups of age, grade, IDH mutation, and 1p/19q co-deletion status in the TCGA dataset **B** Subgroup analysis of clinical characteristics: Subgroups of age, grade, IDH mutation and 1p/19q co-deletion status in the CGGA dataset **C** The MRGs-based nomogram was constructed to predict the OS of LGG patients at 1, 3, and 5 years in the TCGA dataset **D** The calibration plots for the evaluation of predicted OS at 1, 3, and 5 years in the TCGA dataset **E** The ROC curves of the nomogram for OS at 1, 3, and 5 years in the analysis of the TCGA dataset **F** The MRGs-based nomogram was constructed to predict the OS of LGG patients at 1, 3, and 5 years in the CGGA dataset **G** The calibration plots for the evaluation of predicted OS at 1, 3, and 5 years in the CGGA dataset **H** Time-dependent ROC curves measuring the predictive value of the MiAS in the CGGA dataset based on the nomogram

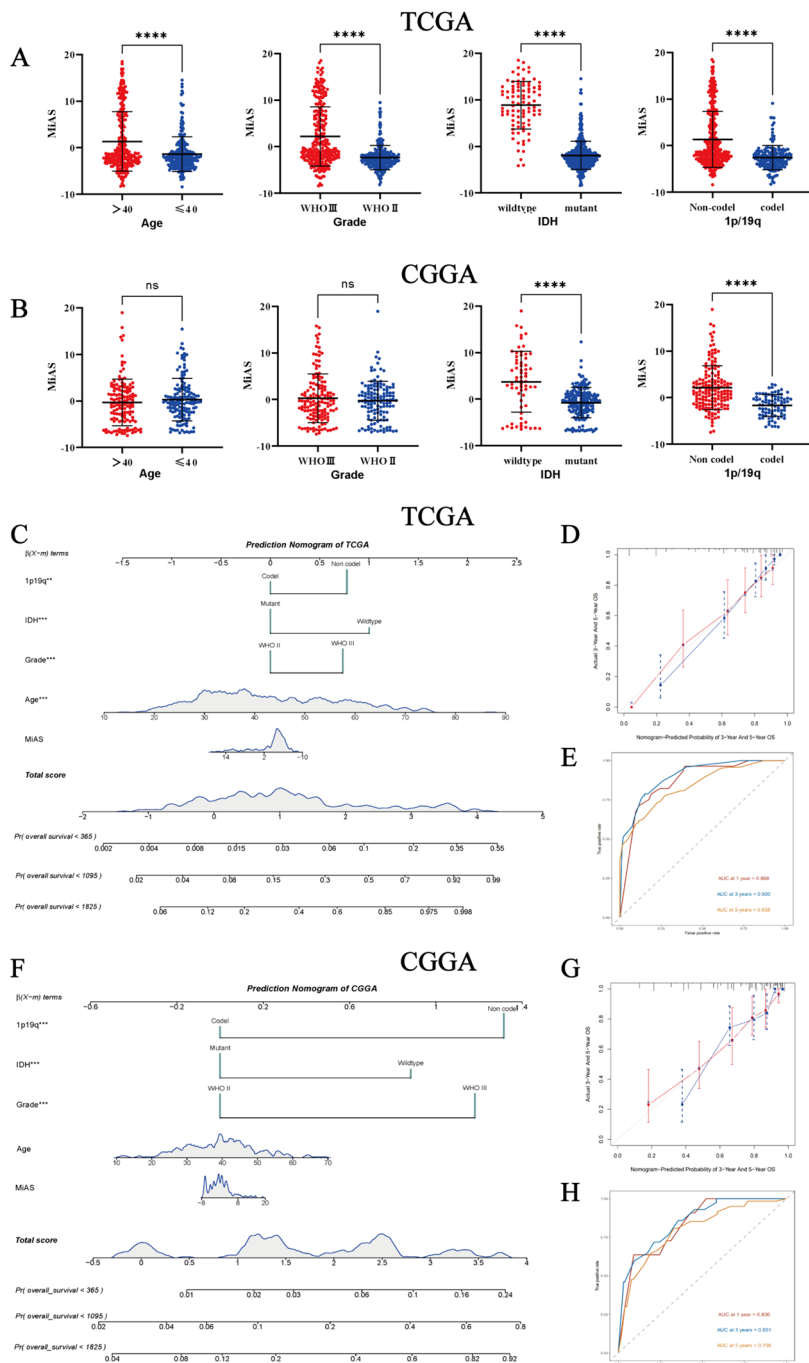
lower sensitivity scores in the high-MiAS group indicated that prognostic scores of Patients could benefit more from 3 drugs AZD6482, MG-132, PLX-4720.

In Vitro Validation of the Relationship between OCIAD2 and LGG

We selected OCIAD2 and performed a series of experiments to validate the role of OCIAD2 in glioma cells. After transfection with lentivirus, we performed qPCR to assess the efficiency of OCIAD2 knockdown and overexpression in cells (Fig. 10A). CCK8 assay and colony formation assay showed that knockdown of OCIAD2 significantly inhibited the proliferation and colony forming ability of glioma cells, whereas overexpression of OCIAD2 enhanced the proliferation and colony forming ability of glioma cells (Fig. 10B, C). Transwell assay showed that knockdown of OCIAD2 inhibited the invasive ability of glioma cells, while overexpression of OCIAD2 enhanced the invasive ability of glioma cells (Fig. 10D). In addition, the results of wound healing assay showed that knockdown of OCIAD2 inhibited the migration ability of glioma cells (Fig. 10E, F). In conclusion, our findings reflect the effect of OCIAD2 on glioma cell phenotype and indicate the predictive role of this novel mitochondrial-related gene signature in the prognosis of LGG patients.

Discussion

Mitochondria are widely involved in a variety of biological processes, such as affecting oxidative stress, cellular metabolism and signal transduction pathways, and participating in apoptosis, playing important biological roles (Nunnari and Suomalainen 2012). Compared to single molecular markers, multigene biomarkers are more accurate and sensitive in terms of predictive ability. In this study, 12 MRGs most associated with prognosis in LGG were identified, and a MiAS model was developed based on these 12 MRGs, which had good results in predicting the prognosis of LGG patients with IDH mutations and 1p/19q co-deletions. Kaplan–Meier curves also showed that patients in the high-MiAS group had significantly shorter OS, which helped to improve LGG patient management and provide decision guidance for the selection of treatment options. In addition, MRGs features have relatively better sensitivity and specificity as independent prognostic predictors compared to traditional clinicopathological features. In this study, a prognostic nomogram based



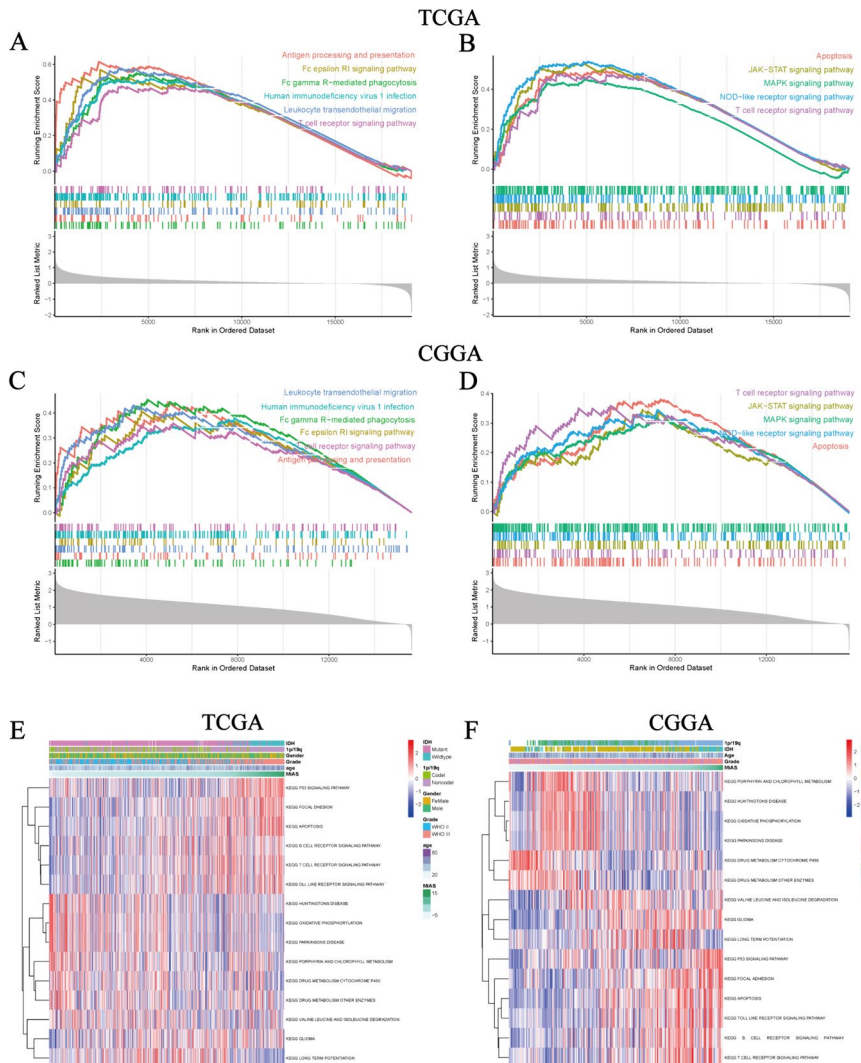


Fig. 5 Functional enrichment analysis between the high-MiAS and low-MiAS groups based on the KEGG pathways **A–D** GSEA results of KEGG pathways in TCGA and CGGA **E–F** GSVA results of KEGG pathways in TCGA and CGGA

on MRGs features with strong AUC values was constructed, and MRGs features could accurately distinguish patients with poor prognosis under different stratification of clinical variables.

After univariate Cox regression analysis and LASSO regression analysis, 12 MRGs with the strongest relationship with prognosis were screened, SLC25A45, ACSS3, UNG, OCIAD2, POLQ, CYP27B1, and MGME1 were highly expressed in the high-MiAS group, while GCAT, ACSL6, CYP24A1, COMTD1 and PRSS35

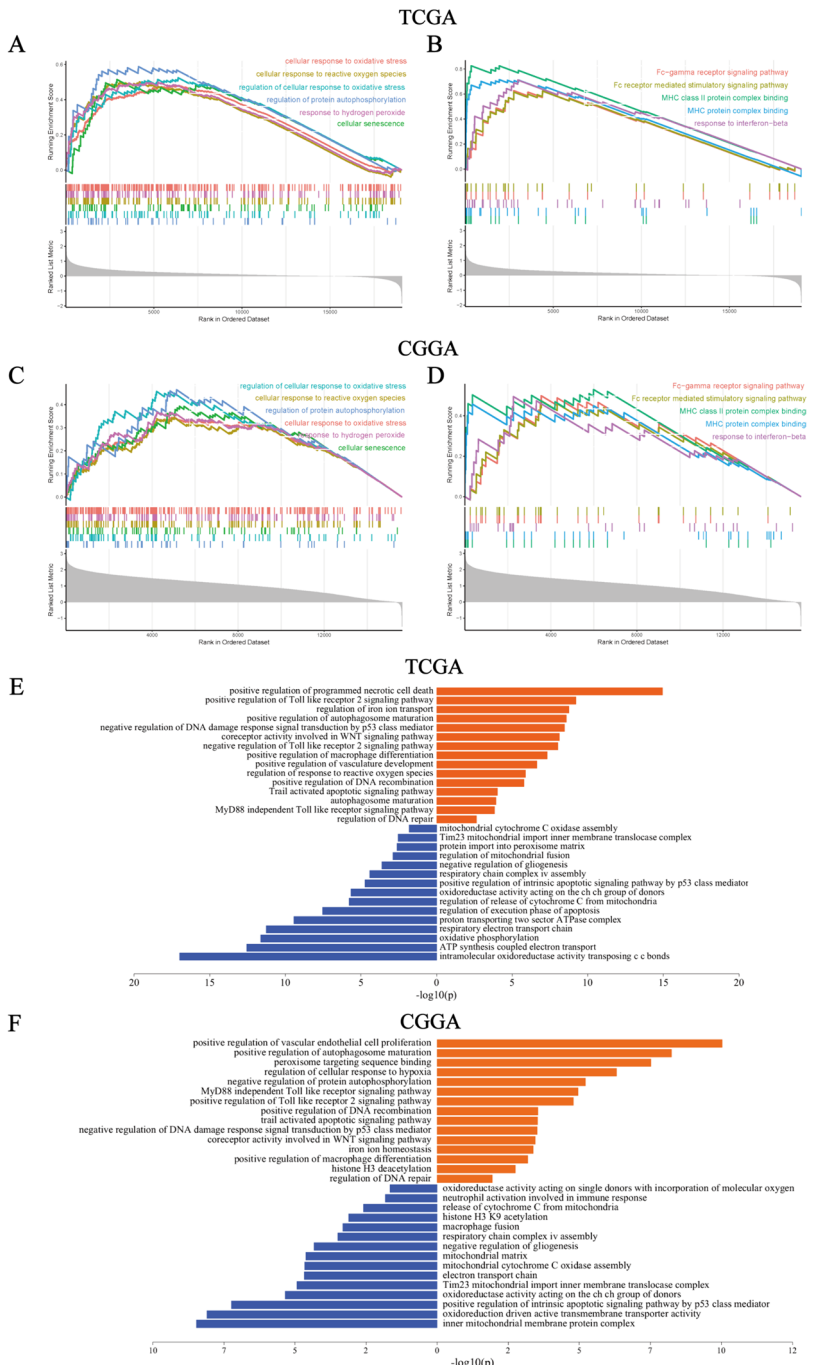


Fig. 6 Enrichment analysis between the high-MiAS and low-MiAS groups based on Gene Ontology (GO). **A–D** GSEA results of GO pathways in TCGA and CGGA. **E, F** GSVA results of GO pathways in TCGA and CGGA

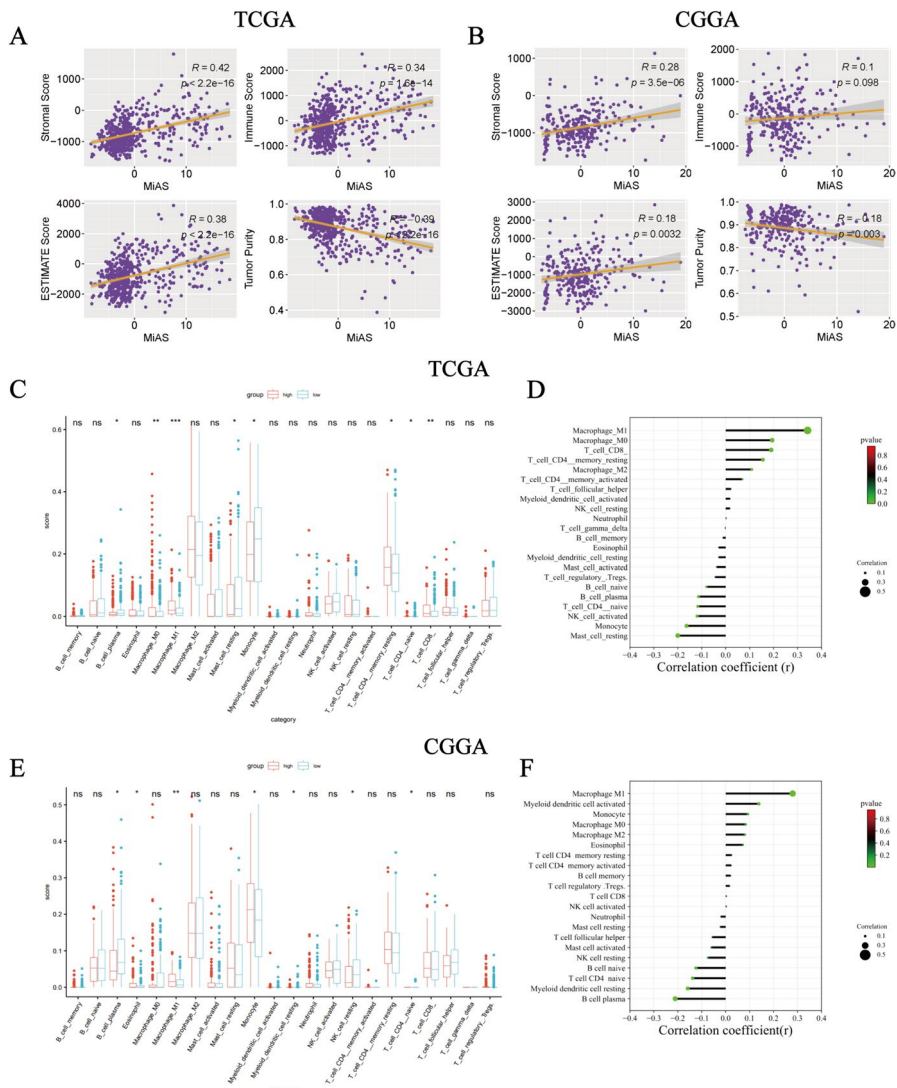


Fig. 7 Comparison of tumor microenvironment (TME) between the high-MiAS and low-MiAS groups **A** The statistical analyses of the stromal score, immune score, ESTIMATE score, and tumor purity between the high-MiAS and low-MiAS groups in the TCGA dataset **B** The statistical analyses of the stromal score, immune score, ESTIMATE score, and tumor purity between the high-MiAS and low-MiAS groups in the CGGA dataset **C** The analysis of immune cells between high-MiAS and low-MiAS groups in the TCGA dataset **D** The correlation coefficient between MiAS and immune cells in the TCGA dataset **E** The analysis of immune cells between high-MiAS and low-MiAS groups in the CGGA dataset **F** The correlation coefficient between MiAS and immune cells in the CGGA dataset

were lowly expressed in the high-MiAS group. Among them, UNG, OCIAD2, CYP24A1, and CYP27B1 have been reported to be associated with glioma. For example, UNG is a uracil DNA glycosylase and one study found that the knockdown

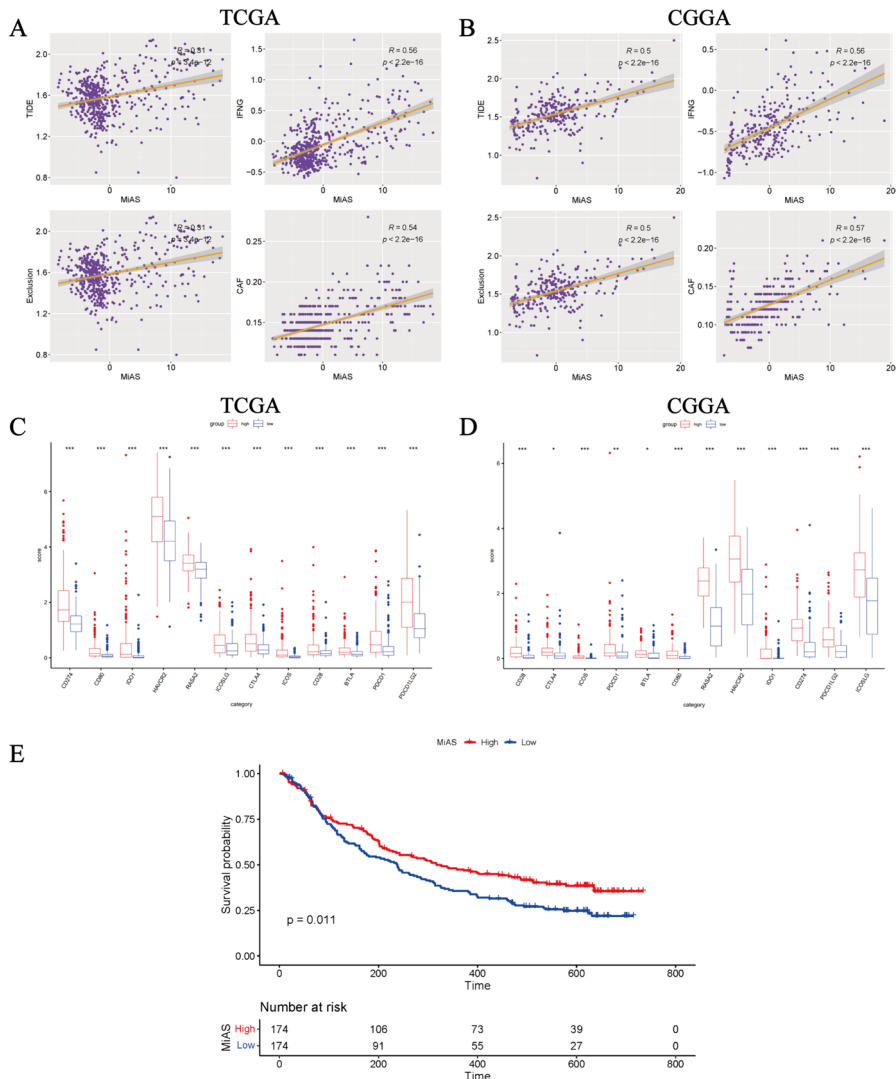


Fig. 8 Correlation between immunotherapy and MiAS **A, B** Correlation between TIDE results and MiAS in TCGA and CGGA **C, D** Expression of 12 immune checkpoints in TCGA and CGGA **E** Survival analysis between high-MiAS and low-MiAS groups in the dataset of patients taking atezolizumab for urothelial carcinoma extracted from the IMvigor210 dataset

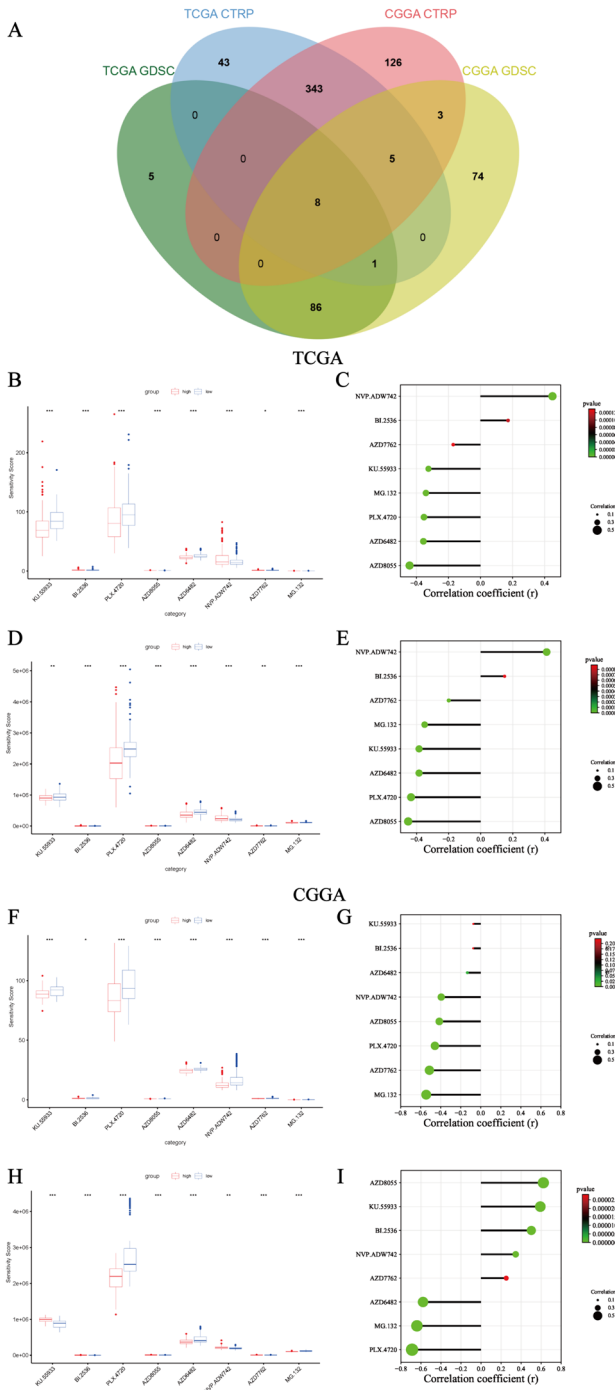
of this gene enhanced the sensitivity of GBM to TMZ (Svilar et al. 2012). OCIAD2 is a novel complex III-specific assembly factor in mitochondria that is dysregulated in gliomas (Chojnacka et al. 2022). One study found that the acidosis-CYP24A1-vitamin D pathway enhances self-renewal and mitochondrial respiration in stem cell-like glioma cells (Hu et al. 2019). Endogenous expression of CYP27B1 and the emergence of selective splicing variants reveal new features of the molecular

Fig. 9 The evaluation of treatment responses by the novel prognosis score based on MRGs signature A ► Venn diagram showing the overlapping drugs between the GDSC2 and CTRP datasets in both TCGA and CGGA **B–E** Screening process of potential drugs based on TCGA **F–I** Screening process of potential drugs based on CGGA

pathogenesis of glioblastoma and may become a new target for glioma therapy (Maas et al. 2001). Similarly, the association of ACS3, ACSL6, POLQ, and PRSS35 with cancer has also been reported (Decock et al. 2012; Schrempf et al. 2021; Yang et al. 2021). In addition, these 12 genes were all found to be associated with LGG prognosis for the first time, which deserves further investigation. In our study, GSEA and GSVA analyses further revealed that these 12 MRGs may affect redox homeostasis, immune infiltration, metastatic mechanisms, and programmed cell death in LGG. These results suggest that these MRGs play an important role in many tumors and may be involved in LGG genesis and progression. To lay the foundation and provide direction for future studies, we selected OCIAD2 and investigated the effect of this gene on the proliferation, clone formation, invasion, and migration ability of glioma cells, whereas the specific functions and molecular mechanisms of other MRGs in LGG are expected to be discovered in future studies.

Studies have shown that the immune microenvironment is closely related to the development of LGG (Yin et al. 2020). Also, mitochondria are closely related to immunity, connecting various metabolic pathways in every immune cell subpopulation from T cells to macrophages (Klein et al. 2020; Breda et al. 2019). It has been suggested that M1 macrophages may induce tumorigenesis by altering the microenvironment, and in the same way as the Warburg effect in tumor cells, immune cells have the ability to shift from oxidative phosphorylation to aerobic glycolysis in order to generate as many metabolic resources as possible to meet the demands of cell proliferation, which is closely linked to macrophage polarization toward M1 (Orihuela et al. 2016). In the present study, macrophage M1 infiltration was significantly increased in the high-MiAS group, which may account for the poor prognosis in the high-MiAS group. Plasma cells are effector cells of the humoral adaptive immune system and may produce tumor antigen-specific antibodies that trigger antibody-dependent cytotoxic responses and activate complement, and enhanced immunoglobulin synthesis is accompanied by a decrease in their mitochondrial content and activity, which explains the enrichment of B-cell plasma in the low-MiAS group (Jang et al. 2015; Sandoval et al. 2018). In a study revealing immune cell infiltration and immunotherapy in low-grade gliomas, high ICI scores were significantly associated with elevated levels of CD4 naïve T-cell infiltration, suggesting that CD4 naïve T cells are associated with a good patient prognosis (Yang et al. 2022), and the enrichment of CD4 naïve T cells in the low-MiAS group in the present study with a good patient prognosis is consistent with the above study. In conclusion, elevated immunosuppression and pro-carcinoma-related immune cell infiltration in the high-MiAS group with reduced anti-glioma immune cell infiltration may be responsible for their poor prognosis.

Gliomas present a significant immunosuppressive microenvironment within gliomas, which is an important cause of poor glioma prognosis. Activation of the



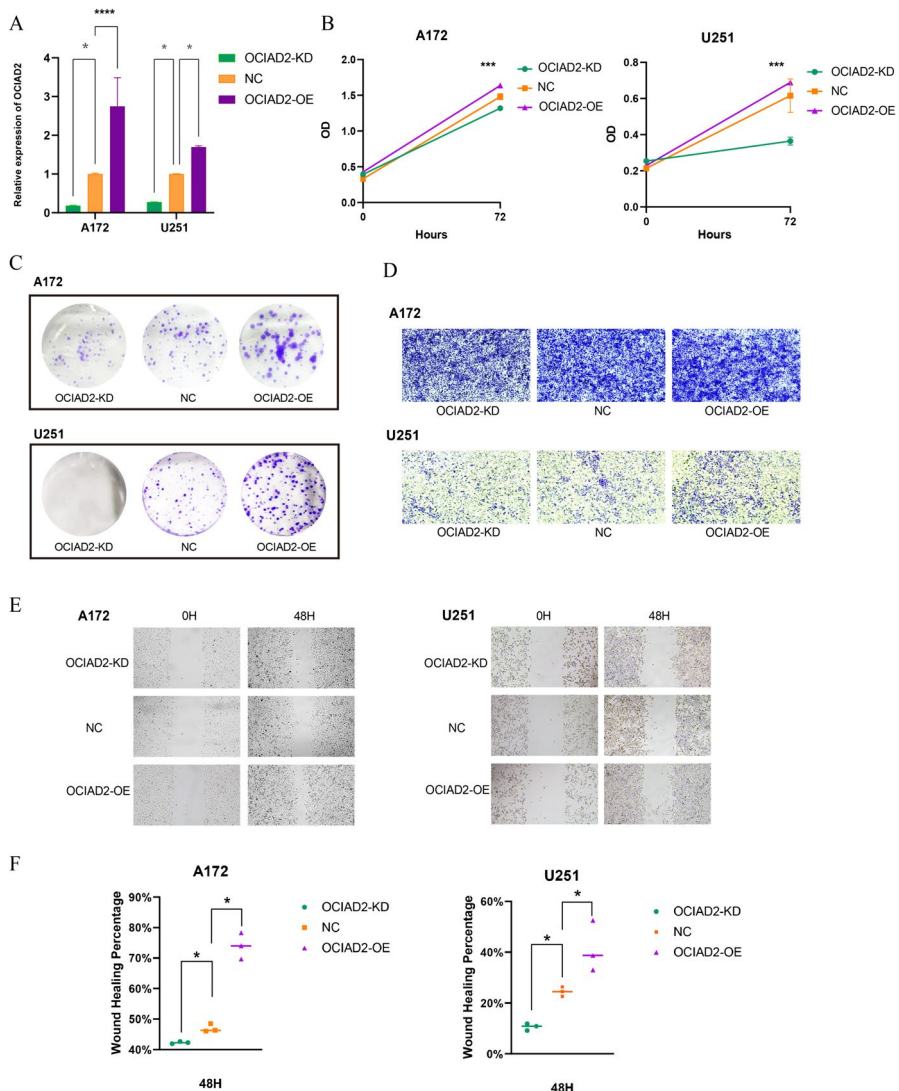


Fig. 10 The relationship between OCIAD2 and LGG was verified in vitro **A** qPCR showing the knockdown and overexpression efficiencies of OCIAD2 in the cells **B** CCK8 assay showing the effect of knockdown and overexpression of OCIAD2 on the proliferation of A172 and U251 cells **C** Colony formation assay showing the effect of knockdown and overexpression of OCIAD2 on the clone forming ability of A172 and U251 cells **D** Transwell showing the effect of knockdown and overexpression of OCIAD2 on the invasion ability of A172 and U251 cells **E, F** Wound healing assay showing the effect of knockdown and overexpression of OCIAD2 on the migration ability of A172 and U251 cells

immune response within gliomas by immunotherapy is one of the most promising and promising means to attack gliomas in the future (Billan et al. 2020). However, due to tumor heterogeneity and individual differences, LGG patients respond differently to immune checkpoint inhibitors (ICIs); therefore, the development of

predictive biomarkers to assess the responsiveness of patients to ICIs would help to individualize the treatment of LGG patients (Zhang et al. 2022). The results of this study showed that the expression of several immune checkpoints was significantly higher in the high-MiAS group than in the low-MiAS group. The TIDE algorithm predicts the response to ICIs by describing the levels of dysfunctional T cells and infiltrating cytotoxic T lymphocytes, and a higher TIDE score indicates a poor tumor response to ICIs (Jiang et al. 2018). According to TIDE results, MiAS was positively correlated with infiltration of CAFs, which was associated with the immunosuppressive tumor microenvironment (Kalluri 2016). In the low-MiAS group, TIDE scores were significantly lower and patient survival was significantly longer, suggesting that MiAS has predictive value in assessing the response of LGG patients to immunotherapy and that LGG patients in the low-MiAS group responded better to immunotherapy. In the IMvigor210 dataset, MiAS was significantly associated with the prognosis of patients with uroepithelial carcinoma treated with anti-PD-L1, and high-MiAS scores had a better prognosis. It has been shown that the presence of follicular helper T cells is necessary for the efficacy of anti-PD-1 therapy (Niogret et al. 2021), and PD-L1 antibodies have theoretically similar anti-tumor mechanisms to PD-1 antibodies (Jiang et al. 2019). According to our findings, the high degree of follicular helper T-cell infiltration in patients in the high-MiAS group may explain the better prognosis of the high-MiAS group in the IMvigor210 dataset. This result suggests that some ICIs may also have good efficacy in LGG patients in the high-MiAS group, and further clinical trials could be conducted accordingly in the future.

Chemotherapy is one of the important treatments for glioma, and temozolomide (TMZ) is the first-line drug for the treatment of malignant glioma (Fukushima et al. 2009). However, the efficacy of TMZ remains suboptimal for gliomas that selectively penetrate the blood–brain barrier and are TMZ-resistant, and the development of alternative chemotherapeutic agents for LGG is of great clinical importance (Lang et al. 2021). The results of this study suggest that AZD6482, MG-132, and PLX-4720 may be potential agents for the treatment of patients in the high-MiAS group, as MiAS was positively correlated with the sensitivity of these agents. Their therapeutic effects on glioma have been demonstrated, such as the phosphatidylinositol-3 kinase inhibitor AZD6482, which effectively inhibits glioma cell proliferation and induces apoptosis (Xu et al. 2019). MG-132 is a proteasome inhibitor that induces apoptosis in C6 glioma cells through oxidative stress (Fan et al. 2011). The BRAF inhibitor PLX-4720 inhibits the growth of glioma cells regardless of BRAF mutation status. Based on the results of this study, MG-132 is particularly recommended for the treatment of patients with high-MiAS scores because MG-132 has the highest sensitivity and is positively correlated with MiAS.

However, there are some limitations in our study. Firstly, our model is based on retrospective analysis and needs to be validated in prospective studies. Additionally, other genes with prognostic value were not considered in our study. Moreover, this study is mainly based on the analysis of bioinformatics technology, but the functional mechanisms and interactions of genes are very complex, and more experimental data are needed for validation and evaluation. In addition, the sensitizing drugs proposed in this study need to be validated in both laboratory and clinical trials.

Conclusion

In this study, we developed a new prognostic signature based on MRGs for anticipating the prognosis of LGG patients, assessing immunotherapy efficacy, and predicting potential drugs. This will enrich the therapeutic strategies for LGG patients and provide some guidance for clinical practice from the perspective of targeting mitochondria.

Supplementary Information The online version contains supplementary material available at <https://doi.org/10.1007/s10528-024-10928-w>.

Acknowledgements Not applicable.

Author Contributions Xiong conceived, designed, and supervised the study. Yang, Shen, and Wu drafted the manuscript. Zhao, Yixuan Zhou, Mei, and Xu collected the data. Wang, Chai, and Cai performed data analysis and visualization. Yang, Jiabin Zhou, Lei, and Yue conducted an experimental verification. All authors contributed to the article and approved the submitted version.

Funding This study did not receive any funding.

Availability of Data and Materials The dataset TCGA-LGG for this study can be found in the GDC database (<https://portal.gdc.cancer.gov/>). The dataset CGGA-LGG for this study can be found in the CGGA database (<http://www.cgga.org.cn/>). The dataset GDSC2 can be found in the GDSC database (<https://www.cancerxgene.org/>). The dataset CTRP v2 can be found in the CTRP database (<https://portals.broadinstitute.org/ctrp/>).

Declarations

Conflict of interest The authors declare that the research was conducted in the absence of any commercial or financial relationships that could be construed as a potential conflict of interest.

Ethical Approval Not applicable.

Consent to Participate Not applicable.

Consent for Publication Not applicable.

References

- Benitez JC, Remon J, Besse B (2020) Current panorama and challenges for neoadjuvant cancer immunotherapy. *Clin Cancer Res* 26(19):5068–5077
- Billan S, Kaidar-Person O, Gil Z (2020) Treatment after progression in the era of immunotherapy. *Lancet Oncol* 21(10):e463–e476
- Breda C, Davanzo GG, Basso PJ, Saraiva CN, Moraes-Vieira P (2019) Mitochondria as central hub of the immune system. *Redox Biol* 26:101255
- Chen X, Fu G, Li L, Zhao Q, Ke Z, Zhang R (2022) Selenoprotein GPX1 is a prognostic and chemotherapy-related biomarker for brain lower grade glioma. *J Trace Elem Med Biol* 74:127082
- Chojnacka KJ, Elancheliyan P, Mussulini B, Mohanraj K, Callegari S, Gosk A et al (2022) Ovarian carcinoma immunoreactive antigen-like protein 2 (OCIAD2) is a novel complex III-specific assembly factor in mitochondria. *Mol Biol Cell* 33(4):ar29

- Decock A, Ongenaert M, Hoebeeck J, De Preter K, Van Peer G, Van Criekinge W et al (2012) Genome-wide promoter methylation analysis in neuroblastoma identifies prognostic methylation biomarkers. *Genome Biol* 13(10):R95
- Fan WH, Hou Y, Meng FK, Wang XF, Luo YN, Ge PF (2011) Proteasome inhibitor MG-132 induces C6 glioma cell apoptosis via oxidative stress. *Acta Pharmacol Sin* 32(5):619–625
- Fukushima T, Takeshima H, Kataoka H (2009) Anti-glioma therapy with temozolomide and status of the DNA-repair gene MGMT. *Anticancer Res* 29(11):4845–4854
- Gene ontology consortium: going forward. *Nucleic Acids Res*. 2015;43(Database issue):D1049–D1056
- Ghandi M, Huang FW, Jane-Valbuena J, Kryukov GV, Lo CC, McDonald ER et al (2019) Next-generation characterization of the cancer cell line encyclopedia. *Nature* 569(7757):503–508
- Hanzelmann S, Castelo R, Guinney J (2013) GSVA: gene set variation analysis for microarray and RNA-seq data. *BMC Bioinform* 14:7
- Hu P, Li S, Tian N, Wu F, Hu Y, Li D et al (2019) Acidosis enhances the self-renewal and mitochondrial respiration of stem cell-like glioma cells through CYP24A1-mediated reduction of vitamin D. *Cell Death Dis* 10(1):25
- Jang KJ, Mano H, Aoki K, Hayashi T, Muto A, Nambu Y et al (2015) Mitochondrial function provides instructive signals for activation-induced B-cell fates. *Nat Commun* 6:6750
- Jiang P, Gu S, Pan D, Fu J, Sahu A, Hu X et al (2018) Signatures of T cell dysfunction and exclusion predict cancer immunotherapy response. *Nat Med* 24(10):1550–1558
- Jiang Y, Chen M, Nie H, Yuan Y (2019) PD-1 and PD-L1 in cancer immunotherapy: clinical implications and future considerations. *Hum Vacc Immunother* 15(5):1111–1122
- Kalluri R (2016) The biology and function of fibroblasts in cancer. *Nat Rev Cancer* 16(9):582–598
- Kanehisa M, Goto S (2000) KEGG: kyoto encyclopedia of genes and genomes. *Nucleic Acids Res* 28(1):27–30
- Klein K, He K, Younes AI, Barsoumian HB, Chen D, Ozgen T et al (2020) Role of mitochondria in cancer immune evasion and potential therapeutic approaches. *Front Immunol* 11:573326
- Lang F, Liu Y, Chou FI, Yang C (2021) Genotoxic therapy and resistance mechanism in gliomas. *Pharmacol Therapeut* 228:107922
- Lapointe S, Perry A, Butowski NA (2018) Primary brain tumours in adults. *Lancet* 392(10145):432–446
- Li S, Wang W, Zi J, Sun M, Mei W, Yang N et al (2020) Elevated expression of mitochondrial transcription elongation factor (TEFM) predicts poor prognosis in low grade glioma—an analysis of the Cancer Genome Atlas (TCGA) dataset. *Transl Cancer Res* 9(5):3610–3622
- Liang BC, Hays L (1996) Mitochondrial DNA copy number changes in human gliomas. *Cancer Lett* 105(2):167–173
- Louis DN, Perry A, Wesseling P, Brat DJ, Cree IA, Figarella-Branger D et al (2021) The 2021 WHO classification of tumors of the central nervous system: a summary. *Neuro Oncol* 23(8):1231–1251
- Maas RM, Reus K, Diesel B, Steudel WI, Feiden W, Fischer U et al (2001) Amplification and expression of splice variants of the gene encoding the P450 cytochrome 25-hydroxyvitamin D(3) 1, alpha-hydroxylase (CYP 27B1) in human malignant glioma. *Clin Cancer Res* 7(4):868–875
- Maeser D, Gruener RF, Huang RS (2021) oncoPredict: an R package for predicting in vivo or cancer patient drug response and biomarkers from cell line screening data. *Brief Bioinform* 22(6)
- Newman AM, Liu CL, Green MR, Gentles AJ, Feng W, Xu Y et al (2015) Robust enumeration of cell subsets from tissue expression profiles. *Nat Methods* 12(5):453–457
- Niogret J, Berger H, Rebe C, Mary R, Ballot E, Truntzer C et al (2021) Follicular helper-T cells restore CD8(+)-dependent antitumor immunity and anti-PD-L1/PD-1 efficacy. *J Immunother Cancer* 9(6)
- Nunnari J, Suomalainen A (2012) Mitochondria: in sickness and in health. *Cell* 148(6):1145–1159
- Ordys BB, Launay S, Deighton RF, McCulloch J, Whittle IR (2010) The role of mitochondria in glioma pathophysiology. *Mol Neurobiol* 42(1):64–75
- Orihuela R, McPherson CA, Harry GJ (2016) Microglial M1/M2 polarization and metabolic states. *Br J Pharmacol* 173(4):649–665
- Poff A, Koutnik AP, Egan KM, Sahebjam S, D'Agostino D, Kumar NB (2019) Targeting the Warburg effect for cancer treatment: Ketogenic diets for management of glioma. *Semin Cancer Biol* 56:135–148
- Rosenberg JE, Hoffman-Censits J, Powles T, van der Heijden MS, Balar AV, Necchi A et al (2016) Atezolizumab in patients with locally advanced and metastatic urothelial carcinoma who have progressed following treatment with platinum-based chemotherapy: a single-arm, multicentre, phase 2 trial. *Lancet* 387(10031):1909–1920

- Sandoval H, Kodali S, Wang J (2018) Regulation of B cell fate, survival, and function by mitochondria and autophagy. *Mitochondrion* 41:58–65
- Schiff D, Van den Bent M, Vogelbaum MA, Wick W, Miller CR, Taphoorn M et al (2019) Recent developments and future directions in adult lower-grade gliomas: Society for Neuro-Oncology (SNO) and European Association of Neuro-Oncology (EANO) consensus. *Neuro Oncol* 21(7):837–853
- Schrempf A, Slyskova J, Loizou JI (2021) Targeting the DNA repair enzyme polymerase theta in cancer therapy. *Trends Cancer* 7(2):98–111
- Seashore-Ludlow B, Rees MG, Cheah JH, Cokol M, Price EV, Coletti ME et al (2015) Harnessing connectivity in a large-scale small-molecule sensitivity dataset. *Cancer Discov* 5(11):1210–1223
- Soffietti R, Baumert BG, Bello L, Von Deimling A, Duffau H, Frenay M et al (2010) Guidelines on management of low-grade gliomas: report of an EFNS-EANO Task Force. *Eur J Neurol* 17(9):1124–1133
- Subramanian A, Tamayo P, Mootha VK, Mukherjee S, Ebert BL, Gillette MA et al (2005) Gene set enrichment analysis: a knowledge-based approach for interpreting genome-wide expression profiles. *Proc Natl Acad Sci USA* 102(43):15545–15550
- Svilar D, Dyavaiah M, Brown AR, Tang JB, Li J, McDonald PR et al (2012) Alkylation sensitivity screens reveal a conserved cross-species functionome. *Mol Cancer Res* 10(12):1580–1596
- van den Bent MJ (2010) Interobserver variation of the histopathological diagnosis in clinical trials on glioma: a clinician's perspective. *Acta Neuropathol* 120(3):297–304
- Wang Z, Dai Z, Zheng L, Xu B, Zhang H, Fan F et al (2021) Ferroptosis activation scoring model assists in chemotherapeutic agents' selection and mediates cross-talk with immunocytes in malignant glioblastoma. *Front Immunol* 12:747408
- Xu PF, Yang JA, Liu JH, Yang X, Liao JM, Yuan FE et al (2019) PI3Kbeta inhibitor AZD6482 exerts anti-proliferative activity and induces apoptosis in human glioblastoma cells. *Oncol Rep* 41(1):125–132
- Yan H, Parsons DW, Jin G, McLendon R, Rasheed BA, Yuan W et al (2009) IDH1 and IDH2 mutations in gliomas. *New Engl J Med* 360(8):765–773
- Yang W, Soares J, Greninger P, Edelman EJ, Lightfoot H, Forbes S et al (2013) Genomics of Drug Sensitivity in Cancer (GDSC): a resource for therapeutic biomarker discovery in cancer cells. *Nucleic Acids Res.* 41(Database issue):D955–D961
- Yang RH, Liang B, Li JH, Pi XB, Yu K, Xiang SJ et al (2021) Identification of a novel tumour microenvironment-based prognostic biomarker in skin cutaneous melanoma. *J Cell Mol Med* 25(23):10990–11001
- Yang Y, Tian Y, Li Q, Jiang R, Zhang J (2022) Uncovering the immune cell infiltration landscape in low-grade glioma for aiding immunotherapy. *J Oncol* 2022:3370727
- Yin W, Jiang X, Tan J, Xin Z, Zhou Q, Zhan C et al (2020) Development and validation of a tumor mutation burden-related immune prognostic model for lower-grade glioma. *FroNt Oncol* 10:1409
- Yoshihara K, Shahmoradgoli M, Martinez E, Vegesna R, Kim H, Torres-Garcia W et al (2013) Inferring tumour purity and stromal and immune cell admixture from expression data. *Nat Commun* 4:2612
- Zhang S, Xiao X, Wang Y, Song T, Li C, Bao H et al (2022) Developing an immune-related signature for predicting survival rate and the response to immune checkpoint inhibitors in patients with glioma. *Front Genet* 13:899125
- Zhao Z, Zhang KN, Wang Q, Li G, Zeng F, Zhang Y et al (2021) Chinese glioma genome atlas (CGGA): a comprehensive resource with functional genomic data from Chinese glioma patients. *Genom Proteom Bioinform* 19(1):1–12

Publisher's Note Springer Nature remains neutral with regard to jurisdictional claims in published maps and institutional affiliations.

Springer Nature or its licensor (e.g. a society or other partner) holds exclusive rights to this article under a publishing agreement with the author(s) or other rightsholder(s); author self-archiving of the accepted manuscript version of this article is solely governed by the terms of such publishing agreement and applicable law.

Authors and Affiliations

Jingyi Yang¹ · Lei Shen¹ · Jiaxin Zhou¹ · Ji Wu¹ · Chuqiao Yue¹ ·
Tiansheng Wang¹ · Songshan Chai¹ · Yuankun Cai¹ · Dongyuan Xu¹ · Yu Lei¹ ·
Jingwei Zhao¹ · Yixuan Zhou¹ · Zhimin Mei¹ · Nanxiang Xiong¹

✉ Nanxiang Xiong
mozhuoxiong@163.com

¹ Department of Neurosurgery, Zhongnan Hospital of Wuhan University, No.169, Donghu Road, Wuhan 430071, Hubei, China